Article

*J. Biol. Regul. Homeost. Agents.* 2024; 38(8): 5733–5742
https://doi.org/10.23812/j.biol.regul.homeost.agents.20243808.460

# Correlation of Zinc Finger Proteins with Immune Infiltration in Gastric Cancer Patients: A Prognostic Signature Model of Five Genes

Pufang Tan[1,2,†], Renshan Hao[2,†], Ye Zhang[3], Qi Zhu[2,4,*], Zhenxin Wang[1,*]

[1]Division of Oncology, The First Affiliated Hospital of Soochow University, 215006 Suzhou, Jiangsu, China
[2]Division of Gastroenterology and Hepatology, Baoshan Branch, Renji Hospital, Shanghai Jiao Tong University School of Medicine, 200444 Shanghai, China
[3]Laboratory of Medicine, Baoshan Branch, Renji Hospital, Shanghai Jiao Tong University School of Medicine, 200444 Shanghai, China
[4]Division of Gastroenterology and Hepatology, Renji Hospital, Shanghai Jiao Tong University School of Medicine, 200127 Shanghai, China
*Correspondence: zhuqidoctor@126.com (Qi Zhu); wangzhenxin@suda.edu.cn (Zhenxin Wang)
[†]These authors contributed equally.
Submitted: 4 February 2024 Revised: 9 March 2024 Accepted: 18 March 2024 Published: 1 August 2024

**Background: Zinc finger (ZNF) proteins play pivotal roles in the initiation, progression, and metastasis of various cancer types. Nevertheless, the precise mechanism of ZNF genes (*ZNFGs*) in the prognosis and treatment of gastric cancer (GC) patients remains unclear.**

**Methods: Transcriptomic data and clinical information related to GC, as well as ZNFG-related data, were retrieved from publicly available databases. Initially, differentially expressed ZNFGs (DE-ZNFGs) were identified through comparative analysis between GC and normal tissue samples. Subsequently, univariate and multivariate regression analyses, and the Least Absolute Shrinkage and Selection Operator (LASSO) algorithm were utilized to identify potential biomarkers and formulate a risk assessment model. Furthermore, Kaplan-Meier survival curve analysis was conducted to analyze the correlation between the risk score and overall survival of GC patients, while the receiver operating characteristic (ROC) curve analysis was performed to evaluate the reliability of the model. Moreover, Gene Set Enrichment Analysis (GSEA) was performed to elucidate Gene Ontology (GO) and Kyoto Encyclopedia of Genes and Genomes (KEGG) enrichment analyses. Finally, comprehensive investigations were conducted to assess immune infiltration, immune checkpoints, and the immunophenoscore of distinct risk groups.**

**Results: A total of 165 DE-ZNFGs were identified, from which, five genes (zinc finger protein 36 (*ZFP36*), zinc finger protein 121 (*ZNF121*), *ZNF131*, *ZNF22*, and Replication initiator 1 (*REPIN1*) were selected as biomarkers to construct the risk model. This model demonstrated high predictive accuracy for the prognosis of GC patients, with an area under the curve (AUC) exceeding 0.6 for 1-, 3- and 5-year survival rates. Both the risk score and patient age were observed to independently predict prognosis in GC. Moreover, GSEA results showed that high risk group exhibited enrichment in pathways related to mitogen-activated protein kinase (MAPK), calcium signaling, neuroregulation, cellular connections, and cytoskeletal regulation, while low risk group was characterized by pathways associated with metabolic processes, transcription of genetic information, and stringent regulation of genetic stability. Immune analysis revealed significantly elevated stromal, immune, and Estimation of STromal and Immune cells in MAlignant Tumors using Expression data (ESTIMATE) composite scores in high-risk patients. Additionally, there was a notable difference in the expression levels of 19 immune cells and 13 immune checkpoints between the two groups, suggesting significant immunological differences.**

**Conclusions: Our ZNFG-related risk model can be used to predict the survival of GC patients and may have potential guiding implications for GC treatment.**

**Keywords:** gastric cancer; zinc finger genes; prognosis; risk model; tumor immune microenvironment

## Introduction

Globally, gastric cancer (GC) ranks as the fifth most prevalent cancer and the fourth highest cause of cancer-related deaths [1]. Despite significant advancements in surgical approaches, radio, and chemotherapy, the overall survival (OS) rate for GC patients, primarily in advanced stages, remains low [2,3]. Currently, the primary method for determining prognosis in clinical settings is the tumor node metastasis (TNM) staging system. However, variations in therapeutic responses and prognoses among patients with cancers of the same stage may occur due to uncharacterized genetic alterations [4]. Existing biomarkers lack the precision to accurately predict patient prognosis. Thus, there is a critical need to identify prognostic indicators capable of reliably forecasting outcomes for individuals with GC.

Journal of
BIOLOGICAL REGULATORS
and Homeostatic Agents

Zinc finger (ZNF) proteins constitute a prominent family of transcription factors characterized by finger-like DNA-binding domains [5]. These proteins play crucial roles in regulating cell proliferation, autophagy, motility, programmed cell death, cellular invasion, DNA maintenance, and chromatin remodeling, all impacting cancer progression [6]. Additionally, ZNF proteins significantly influence immune responses at transcriptional and post-transcriptional levels [7]. Study by Cheng *et al*. [8] has demonstrated that zinc finger homeobox 2 (*ZHX2*) exhibits elevated expression in GC tissues, correlating significantly with clinical characteristics and poor prognosis. Increased *ZHX2* levels in GC are associated with immune cell infiltration, including B cells, CD4+ T cells, macrophages, and dendritic cells. Moreover, the upregulation of *ZHX2* enhances the proliferative, invasive, and migratory capacities of gastric cancer cells while inhibiting apoptosis. Jin *et al*. [9] reported that *ZNF479* promotes GC cell proliferation, glucose uptake, lactate production, adenosine triphosphate levels, extracellular acidification ratios, and tumor growth while decreasing the oxygen consumption ratio through modulation of the $\beta$-catenin/c-Myc signaling pathway. Similarly, *ZNF139* promotes cell proliferation and inhibits apoptosis by upregulating x-IAP, survivin, and Bcl-2 expression and downregulating Bax and caspase-3 levels [10]. Notably, *ZNF139* expression levels are significantly elevated in GC patients, and high *ZNF139* expression independently predicts patient prognosis [11].

Consequently, we constructed a prognostic model based on ZNF genes (*ZNFGs*), employing the Least Absolute Shrinkage and Selection Operator (LASSO) coupled with Cox regression analyses. This predictive model demonstrated clinical utility in estimating the outcomes of GC patients and was intricately associated with immune functionality and the degree of immune cell infiltration.

## Materials and Methods

### *Data Sources*

We retrieved the GC-RNA expression matrix from the Cancer Genome Atlas (TCGA) database (https://xenabrowser.net). This matrix encompassed mRNA data from 375 GC patients and 32 normal samples (NS), along with survival and clinical data from 350 GC patients. Additionally, we acquired the GSE26901 dataset, containing survival information for 109 individuals with GC, from the Gene Expression Omnibus database (https://www.ncbi.nlm.nih.gov/) [12], which served as an external validation dataset. Furthermore, we identified 1057 ZNFGs using the UniProt database (http://www.uniprot.org) by the keyword "Zinc finger protein".

### *Identification and Functional Enrichment Analyses of Differentially Expressed ZNFGs (DE-ZNFGs)*

Initially, we combined the expression matrix of GC patients from the TCGA cohort with the 1057 ZNFGs from UniProt to create a ZNFG expression matrix. Subsequently, we used the "linear models for microarray data" package (v 3.52.4) to identify differentially expressed ZNFGs (DE-ZNFGs) in 375 GC patients and 32 NS from TCGA, employing the following criteria: "adj. $p < 0.05$" and "$|\log_2 \mathrm{FC}| > 0.5$". Finally, DE-ZNFGs were subjected to functional enrichment analyses using the "clusterProfiler" package (v 4.8.3) [13] for Gene Ontology (GO) and Kyoto Encyclopedia of Genes and Genomes (KEGG) pathways.

### *Constructing and Validating the Risk Model*

Initially, univariate Cox analysis [14] was conducted on DE-ZNFGs identified within the TCGA cohort ($p < 0.1$). Subsequently, the "glmnet" package (v 4.1.7) [15] was employed to implement the Least Absolute Shrinkage and Selection Operator (LASSO) algorithm on the DE-ZNFGs, with parameter settings including family = "cox", and n-fold = 20, resulting in the identification of feature DE-ZNFGs. Further, stepwise multivariate Cox analysis was performed on these feature DE-ZNFGs to screen for potential biomarkers. The coefficients of these biomarkers were utilized to construct the risk model. Additionally, we calculated the risk score (RS) for all GC patients in the TCGA cohort using the following formula: $\mathrm{RS} = \sum_{n=1}^{n} coef_i \times x_i$. Subsequently, we stratified the 350 GC patients into a high-risk group (HRG) and a low-risk group (LRG) based on the median RS value.

Moreover, receiver operating characteristic (ROC) curves of the predictive model were plotted, and the corresponding area under the curve (AUC) values were calculated using the "survivalROC" package (v 1.0.3) to assess the accuracy of the model in predicting patient prognosis. Additionally, a risk curve of the risk model and a heatmap of the biomarkers were generated for patients in both groups. Finally, these evaluation procedures were replicated on the external validation set (GSE26901) to assess the applicability of the model.

### *Independent Prognostic Analysis*

We investigated the prognostic predictive potential of our risk model alongside various clinicopathological features. Firstly, univariate Cox analysis was performed on clinicopathological features, including age, gender, pathological T, N, M, tumor stage, neoplasm histological grade, and the RS of 350 GC patients from TCGA ($p < 0.05$). Subsequently, a multivariate Cox analysis was performed on the statistically significant clinicopathological features.

### *Gene Set Enrichment Analysis (GSEA)*

We used the "GSEA" package (v 4.0.3) with the settings "c2.cp.kegg.V7.4.symbols.gmt" and

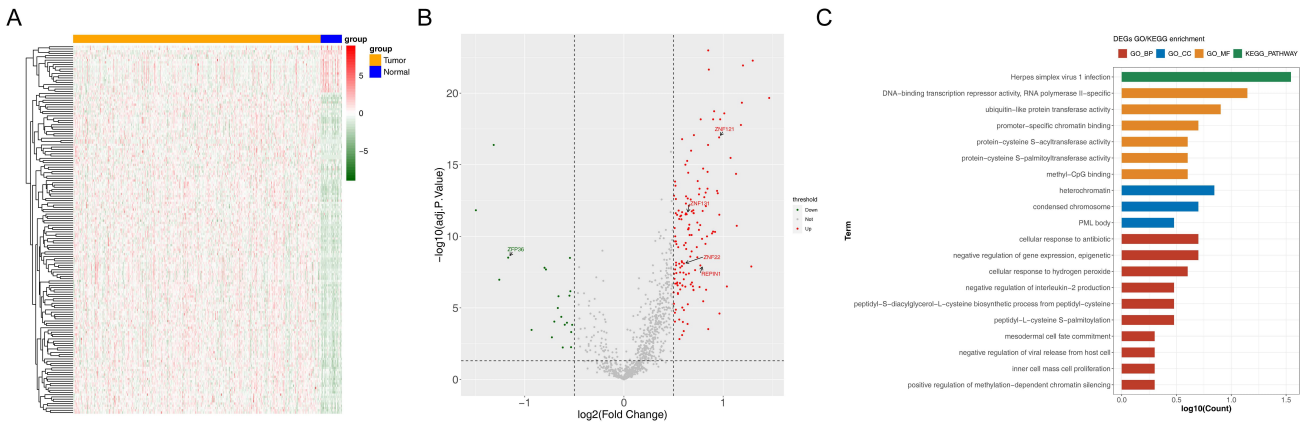


**Fig. 1. Identification of differentially expressed ZNF genes (DE-ZNFGs) in gastric cancer (GC) patients (n = 375) and normal samples (NS) (n = 32) from the Cancer Genome Atlas (TCGA) cohort.** (A) Heatmap illustrating the expression patterns of DE-ZNFGs. (B) Volcano plot showing DE-ZNFGs. (C) Gene Ontology (GO) and Kyoto Encyclopedia of Genes and Genomes (KEGG) analyses of DE-ZNFGs. ZNF, zinc finger.

"c5.go.bp.v7.4.symbols.gmt", using KEGG pathway and GO biological process (BP) as the enrichment background. We identified differentially regulated pathways or functions between the HRG and LRG based on a nominal $p$-value $< 0.05$.

### *Analyzing Tumor Immune Microenvironment (TIME)*

The "Estimation of STromal and Immune cells in MAlignant Tumors using Expression data (ESTIMATE)" algorithm [16] was employed to evaluate variations in immune and stromal scores, and the combined ESTIMATE score among patients from TCGA classified into HRG and LRG. Subsequently, the "ggplot2" package (v 3.3.6) in R was used to visualize results using the Wilcoxon test. Additionally, Spearman correlation analysis was performed to determine the correlation between RS and stromal, immune, and ESTIMATE composite scores. The corresponding $p$-value and correlation coefficient were calculated, and a scatter diagram illustrating the correlation between RS and immune, stromal, and ESTIMATE scores was generated using the "ggplot2" R package.

Furthermore, to quantify the presence of 28 types of immune cells within each sample, we employed the "single set GSEA (ssGSEA)" algorithm. Spearman correlation analysis was then applied to determine the correlation between RS and differentially expressed immune cells. The resulting $p$-values and correlation coefficient were obtained and visualized using the "ggplot2" package.

Subsequently, we extracted the expression levels of immune checkpoints (ADORA2A, CD160, BTLA, KIR2DL3, CD244, PDCD1LG2, CSF1R, TIGIT, HAVCR2, IDO1, IL10RB, IL10, CTLA4, KIR2DL1, CD274, LAG3, KDR, LGALS9, CD96, PVRL2, TGFB1, TGFBR1, PDCD1, and VTCN1) from GC patient in the TCGA cohort. Differential expression of immune checkpoints between LRG and HRG was identified. Finally, the correlation between RS and differential immune checkpoints was determined using the Spearman method.

Furthermore, we evaluated the response of patients in the LRG and HRG to immunotherapy by calculating the immunophenoscore (IPS) of the 350 samples in the TCGA cohort. A boxplot was generated to present a comparison of IPS between both groups.

## Results

### *Identification and Functional Enrichment Analyses of DE-ZNFGs*

A total of 165 DE-ZNFGs were identified, comprising 144 upregulated and 21 downregulated ZNFGs. The heatmap and volcano plot illustrate the distribution and expression levels of these DE-ZNFGs (Fig. 1A,B). Moreover, functional enrichment analyses revealed that these 165 DE-ZNFGs were significantly enriched in 47 GO terms and one KEGG pathway. Among the biological process (BP) terms, the DE-ZNFGs were enriched in 38 terms, including cellular response to antibiotic, negative regulation of gene expression, epigenetic regulation, and cellular response to hydrogen peroxide. The three GO-CC terms enriched by DE-ZNFGs were promyelocytic leukemia (PML) body, condensed chromosome, and heterochromatin. Moreover, the six GO-MF terms enriched by DE-ZNFGs encompassed DNA-binding transcription repression, ubiquitin-like protein transferase activity, promoter-specific chromatin binding, protein-cysteine S-acyltransferase activity, and protein-cysteine S-palmitoyltransferase activity, and methyl-CpG binding. Furthermore, the only KEGG pathway enriched by DE-ZNFGs was herpes simplex virus 1 infection (Fig. 1C). These findings highlight the diverse functional roles of DE-ZNFGs in various biological processes and pathways associated with cancer progression and immune regulation.

Journal of
BIOLOGICAL REGULATORS
and Homeostatic Agents

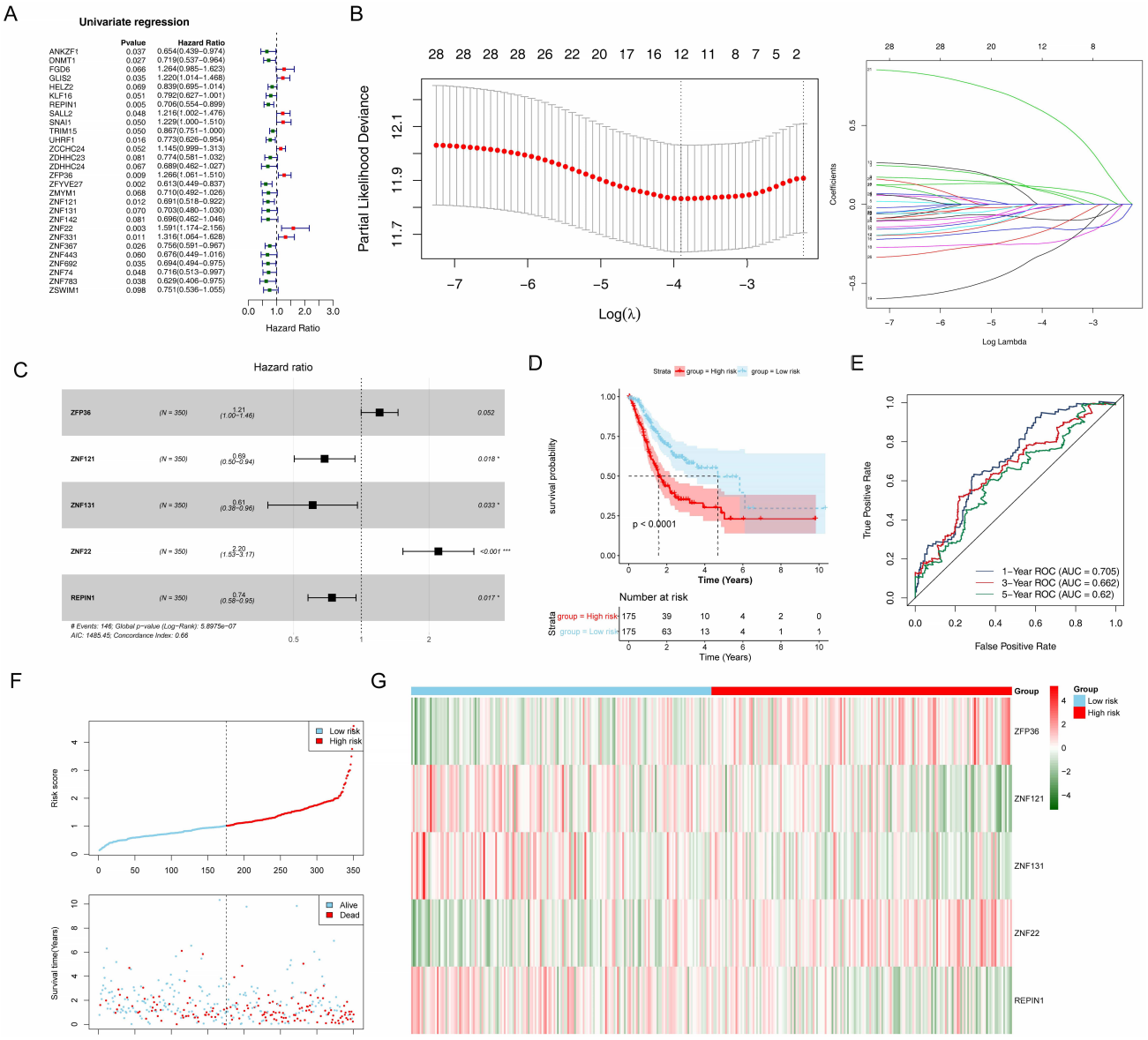


**Fig. 2. Development of a biomarker-based prognostic signature for GC patients in the TCGA cohort.** (A) Univariate Cox analysis screens prognosis-related DE-ZNFGs. (B) Least Absolute Shrinkage and Selection Operator (LASSO) coefficients profile of the prognosis-related DE-ZNFGs. (C) Multivariate Cox analysis identifies the biomarkers. (D) Kaplan-Meier (KM) survival analysis of the high-risk group (HRG) (n = 175) and low-risk group (LRG) (n = 175). (E) Receiver operating characteristic (ROC) curves of risk score (RS) predicting 1-, 3-, and 5-year overall survival (OS). (F) Distribution of survival status of patients in the TCGA cohort. (G) Expression of biomarkers in HRG and LRG. *$p < 0.05$, ***$p < 0.001$.

### *Construction of a ZNFG-Related Prognostic Model*

We initially screened 28 out of the 165 DE-ZNFGs using univariate Cox analysis (Fig. 2A). Subsequently, 12 feature DE-ZNFGs, including *FGD6*, Replication initiator 1 (*REPIN1*), *SNAI1*, *TRIM15*, *ZDHHC24*, zinc finger protein 36 (*ZFP36*), *ZFYVE27*, *ZNF121*, *ZNF131*, *ZNF22*, *ZNF443*, and *ZNF74*, were selected from these 28 DE-ZNFGs using LASSO with the criterion of lambda.min = 0.02020203 (Fig. 2B). Finally, five biomarkers, namely *ZFP36*, *ZNF121*, *ZNF131*, *ZNF22*, and *REPIN1*, were identified using multivariate Cox analysis (Fig. 2C).

The RS was calculated using the following formula: 0.187132798 × *ZFP36* + (–0.376229302) × *ZNF121* + (–0.498680748) × *ZNF131* + 0.789220676 × *ZNF22* + (–0.30051864) × *REPIN1*. Subsequently, based on the median RS value (1.012), we categorized the 350 GC patients into the HRG (175 GC samples) and LRG (175 GC samples). The Kaplan-Meier (KM) survival curve of RS of all patients in both groups revealed that patients in LRG exhibited a significantly better survival rate ($p < 0.0001$) (Fig. 2D). Moreover, AUC values for 1-, 3- and 5-year survival rates all exceeded 0.6, suggesting the effectiveness of our model in accurately forecasting the outcomes

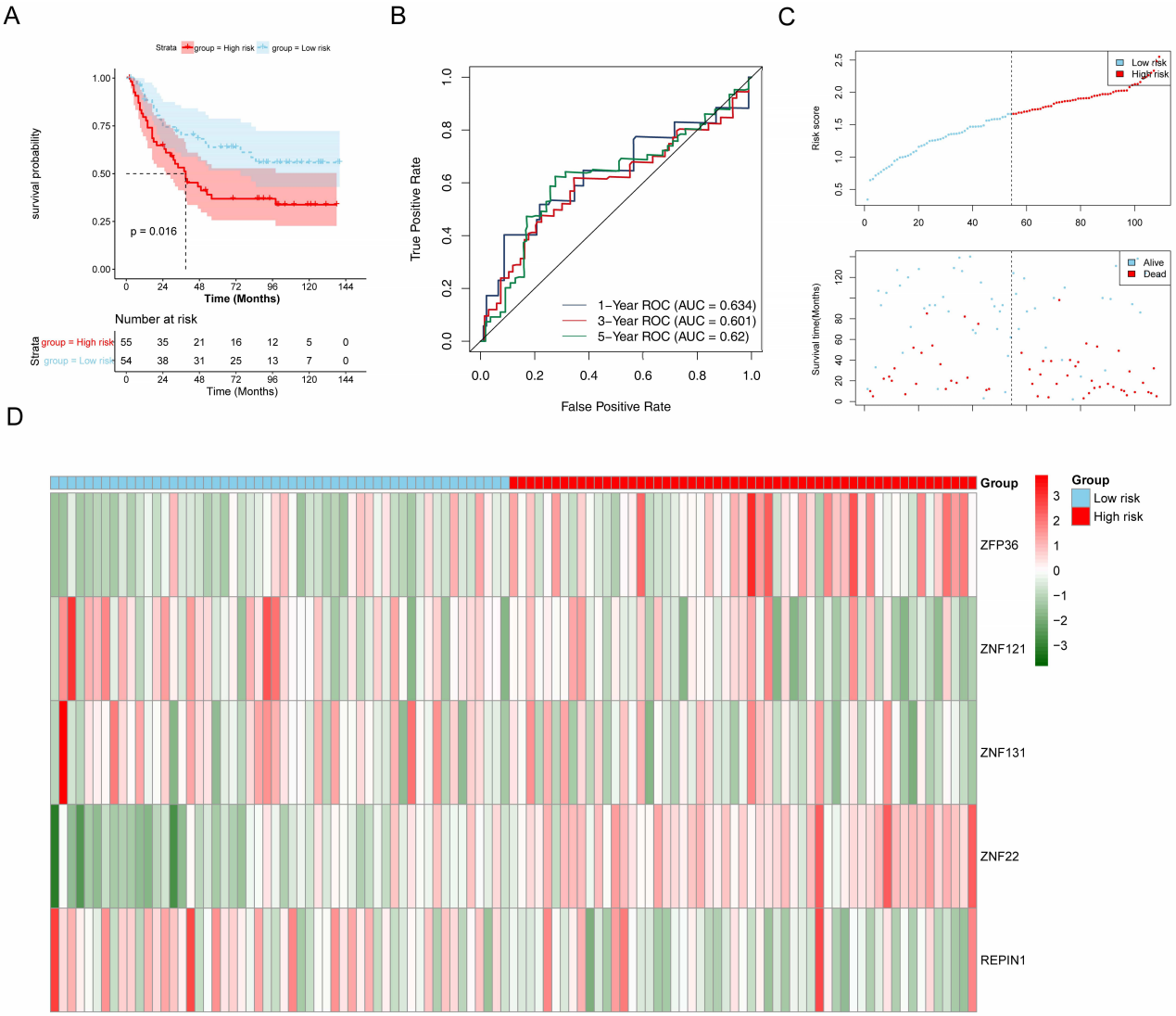


**Fig. 3. Validation of the ZNFG-related prognostic signature in the GSE26901 dataset.** (A) Kaplan-Meier survival curve of the HRG (n = 55) and LRG (n = 54) in the GSE26901 dataset. (B) ROC curves of RS predicting 1-, 3-, and 5-year OS in the GSE26901 dataset. (C) Distribution of survival status of patients in the GSE26901 dataset. (D) Expression of biomarkers in HRG and LRGs in the GSE26901 dataset.

for GC patients (Fig. 2E). The risk profile demonstrated that patients within the HRG had elevated RS and experienced shorter survival time (Fig. 2F). Additionally, the heatmap representation revealed elevated expression levels of *ZFP36* and *ZNF22*, and reduced expression levels of *ZNF121*, *ZNF131*, and *REPIN1* among patients in the HRG (Fig. 2G). This trend aligns with the findings in Fig. 2C, where, within the forest plot analysis, *ZFP36* and *ZNF22* exhibited Hazard Ratios (HRs) exceeding 1, suggesting their roles as risk factors for GC. Conversely, *ZNF121*, *ZNF131*, and *REPIN1*, with HRs below 1, imply their potential roles as protective factors against GC.

Moreover, 109 GC patients from the external validation set (GSE26901) were grouped into HRG (n = 55) and LRG (n = 54) based on median RS (1.667). The ROC curves for the external validation group at 1, 3, and 5 years exhibited AUC values greater than 0.6, aligning with the outcomes observed in the TCGA cohort. These findings suggest that this prognostic model has potential applicability in forecasting patient survival (Fig. 3A–D).

### *Independent Prognostic Analysis*

Results from the univariate Cox analysis indicated that age, pathological T, N, M, tumor stage, and the RS demonstrated significant clinical relevance ($p < 0.05$) (Fig. 4A). Furthermore, multivariate Cox analysis was conducted on these six factors, revealing that patient age and the RS were significant clinicopathological factors ($p < 0.01$) (Fig. 4B).

Journal of
BIOLOGICAL REGULATORS
and Homeostatic Agents

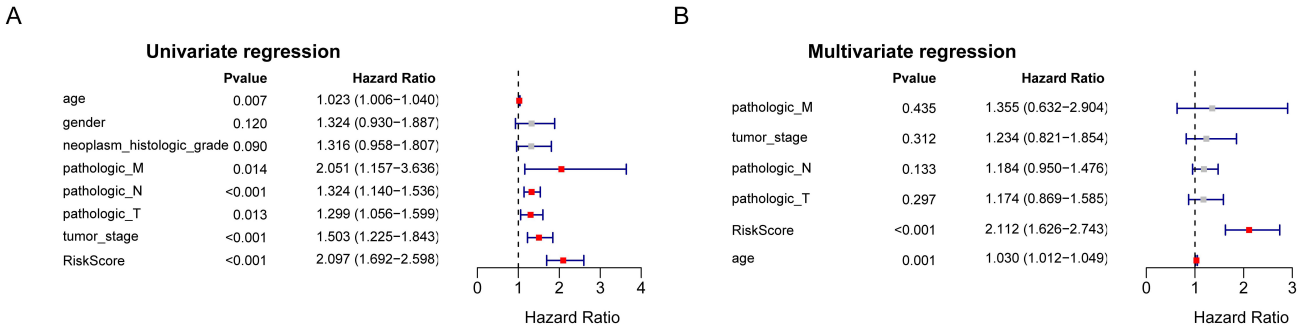


**Fig. 4. ZNFG prognostic signature independently predicts GC patient prognosis in the TCGA cohort.** (A) Univariate and (B) multivariate Cox analyses identify independent prognostic factors.

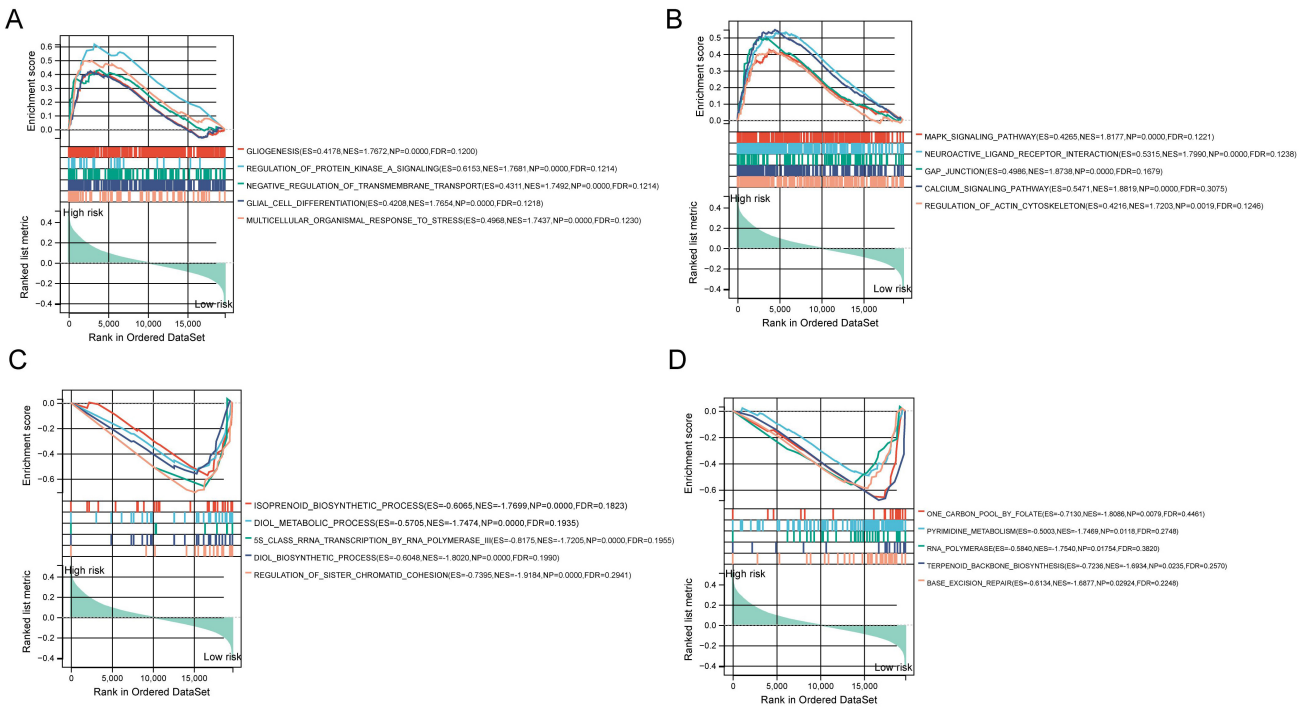


**Fig. 5. Results of Gene Set Enrichment Analysis (GSEA).** (A,B) Top five GO-biological process (BP) terms and KEGG pathways in the HRG (n = 175) (C,D) and the LRG (n = 175).

## *Gene Set Enrichment Analysis (GSEA)*

In the high-risk group (HRG), GO-biological process (BP) terms enriched by genes included gliogenesis, protein kinase A signaling regulation, negative regulation of transmembrane transport, glial cell differentiation, and multicellular organismal response (Fig. 5A). Additionally, KEGG pathways enriched by genes in the HRG encompassed the mitogen-activated protein kinase (MAPK) and calcium signaling pathways, interaction between neuroactive ligand receptors, gap junctions, and actin cytoskeleton regulation (Fig. 5B).

Conversely, in the low-risk group (LRG), GO-BP terms enriched by genes included isoprenoid biosynthetic, diol metabolic and biosynthetic processes, transcription of 5S class rRNA by RNA polymerase III, and regulation of sister chromatid cohesion (Fig. 5C). Furthermore, significantly enriched KEGG pathways in the LRG consisted of the one-carbon pool by folate, pyrimidine metabolism, RNA polymerase, and terpenoid backbone biosynthesis and base excision repair pathways (Fig. 5D).

## *Correlation between the Risk Model and TIME*

The results of ESTIMATE analysis revealed significantly higher stromal, immune, and ESTIMATE composite scores among patients in the HRG ($p < 0.001$) (Fig. 6A). Subsequently, the correlation scatter diagram demonstrated a positive correlation between the RS and stromal as well as ESTIMATE scores ($p < 0.05$ and $r > 0.3$) (Fig. 6B).

Additionally, the ssGSEA boxplot showed a significant difference in 19 immune cell types between both groups, including activated, effector memory, and central memory CD8 T cells, immature and activated B cells,

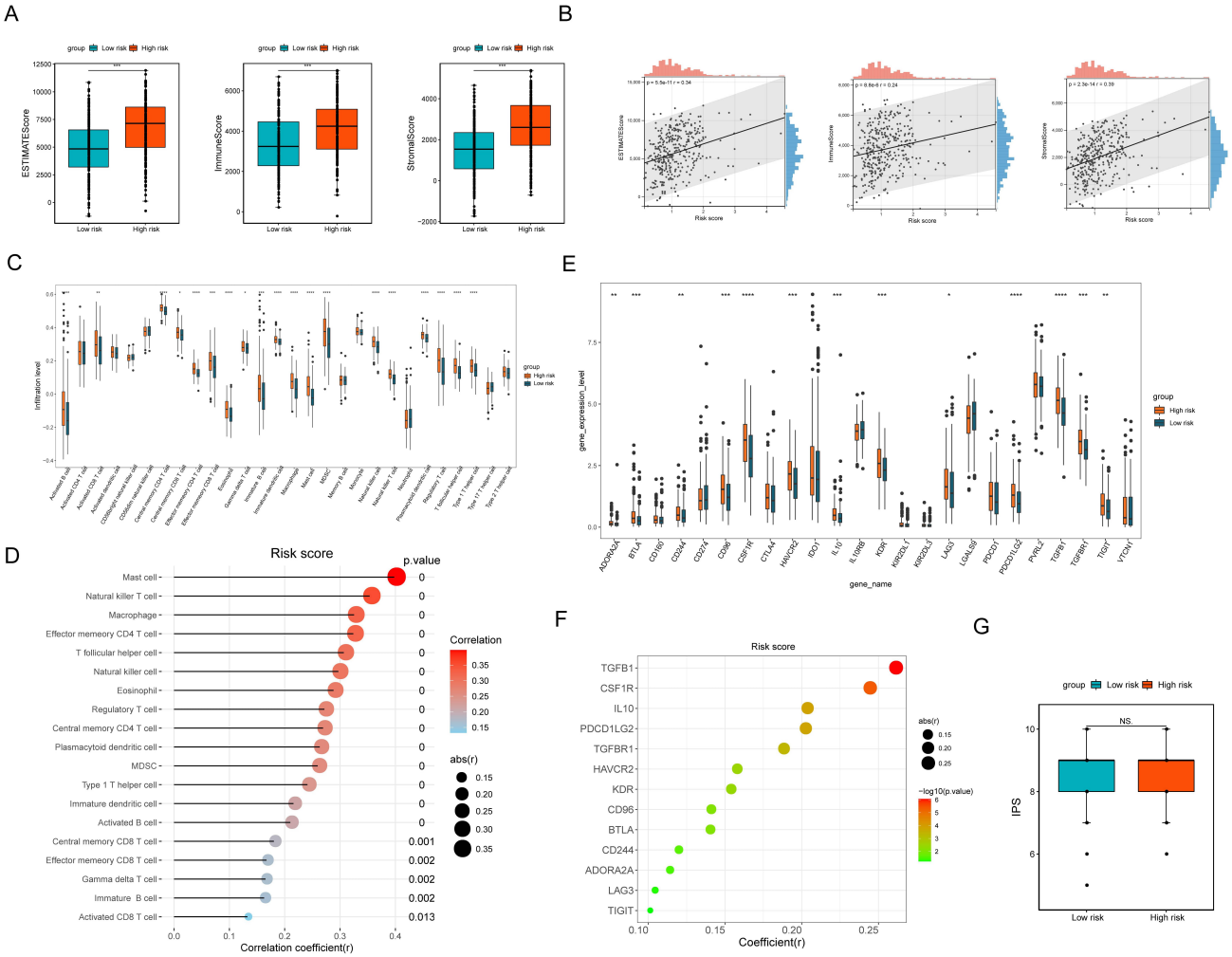


**Fig. 6. Analysis of the Tumor Immune Microenvironment in patients from the TCGA cohort in HRG and LRG.** (A) Differences in stromal, immune, and ESTIMATE composite scores between HRG (n = 175) and LRG (n = 175). (B) Correlation between risk score (RS) and ESTIMATE, immune, and stromal scores. (C) Differences in the infiltration of 28 immune cell types between the two groups. (D) Correlation between the RS and 19 immune cell types. (E) Differences in the expression of 24 immune checkpoints between the two groups. (F) Correlation between the RS and differential immune checkpoints. (G) Differences in the immunophenoscore (IPS) of patients between the two groups. *$p < 0.05$, **$p < 0.01$, ***$p < 0.001$, ****$p < 0.0001$, NS: $p > 0.05$. ESTIMATE, Estimation of STromal and Immune cells in MAlignant Tumors using Expression data.

gamma delta T cells, immature and plasmacytoid dendritic cells, type 1 T helper cells, MDSC, central memory and effector memory CD4 T cells, regulatory T cells, eosinophils, natural killer cells, T follicular helper cells, macrophages, natural killer T (NKT) cells, and mast cells between both groups, all of which were higher in the HRG ($p < 0.05$) (Fig. 6C). The correlation between the RS and mast cells was the strongest, followed by NKT cells, macrophages, and effector memory CD4 T cells, among others (Fig. 6D).

The results also demonstrated differences in the expression of 13 immune checkpoints between both groups, including *ADORA2A*, *CD244*, *TGFB1*, *CSF1R*, *IL10*, *CD96*, *KDR*, *LAG3*, *HAVCR2*, *PDCD1LG2*, *BTLA*, *TGFBR1*, and *TIGIT* ($p < 0.05$), with higher expression level observed among patients in the HRG (Fig. 6E). The correlation results revealed that the RS demonstrated some degree of correlation with these 13 immune checkpoints, with notable emphasis on *TGFB1* and *CSF1R* (Fig. 6F). However, the immunophenoscore (IPS) did not exhibit significant difference between the two groups ($p > 0.05$) (Fig. 6G).

## Discussion

Gastric cancer (GC) is a prevalent malignancy with a steadily increasing annual incidence [17]. Notably, despite similar TNM stages, some GC patients exhibit diverse treatment responses and prognoses [18]. Hence, the identification of precise, accurate, and sensitive biomarkers is imperative for predicting the diagnosis and prognosis of GC patients. Zinc finger genes (ZNFGs) in humans encode the most extensive family of regulatory proteins characterized

Journal of
BIOLOGICAL REGULATORS
and Homeostatic Agents

by zinc ion-binding domains resembling finger-like projections [5]. ZNF proteins, a subset of ZNFGs, are intricately involved in the onset, progression, and metastasis of various cancers.

Through a combination of univariate and multivariate analyses along with LASSO modeling, five ZNFGs were identified, including *ZFP36*, *ZNF121*, *ZNF131*, *ZNF22*, and *REPIN1*, to construct a risk model. *ZFP36*, known as tristetraprolin, is an RNA-binding protein that induces mesenchymal-to-epithelial transition by downregulating Twist1 and Snail1 levels [19]. Several studies have linked *ZFP36* to cancer, noting reduced expression levels in various tumors [20–23]. Chen *et al*. [24] observed decreased *ZFP36* expression in hepatocellular carcinoma tissues compared to adjacent non-tumorous tissues. Furthermore, *ZFP36* has been associated with modulating protein regulators of cytokinesis 1, suppressing cell proliferation, migration, and invasion, and enhancing sensitivity to 5-fluorouracil treatment in xenograft tumor models. Moreover, Chen *et al*. [25] identified a variable pentanucleotide repeat $(ATTTT)_n$ within the 3' untranslated region of the *ZNF121* gene, which encodes a protein of 390 amino acids and has a molecular mass of approximately 43 kDa. Studies have shown that *ZNF121* regulates growth and differentiation of human embryonic stem cells [26,27] and augments the growth and invasiveness in lung and breast cancers [28,29]. *ZNF131,* belonging to the POZ-ZNF protein superfamily, acts as a transcriptional regulator [30]. Huang *et al*. [31] showed that *ZNF131* regulates apyrimidinic endonuclease 1 expression to promote melanoma cell proliferation and migration. *ZNF22*, a classic TF, exhibits significant upregulation in glioblastoma tissues and independently predicts prognosis in glioblastoma patients [32]. Our results indicated that *ZNF22* could independently predict the poor prognosis of GC patients. Replication initiator 1 (*REPIN1*), a ZNF-DNA-binding protein, initiates DNA replication [33,34]. Studies have indicated that *REPIN1* promotes proliferation, migration, and invasion in papillary thyroid carcinoma cells [35], while low expression levels correlate with poor overall survival in glioma patients [36]. Moreover, Hsa-mir-127 inhibits *REPIN1* to enhance the proliferative, migratory, and invasive abilities of glioma cells. However, Qi *et al*. [37] demonstrated that patients with multiple myeloma expressing high levels of *REPIN1* exhibited poor outcomes.

Subsequently, GSEA was performed to determine the underlying mechanism of action of these five ZNFGs in GC. Our findings revealed enrichment of the mitogen-activated protein kinase (MAPK) and calcium signaling pathways in HRG. The MAPK signaling pathway, an evolutionarily conserved signaling pathway [38], regulates cell proliferation, apoptosis, and metabolism, thus contributing to the development of malignant phenotypes [39]. For instance, Du *et al*. [40] suggested that DNA-damage-inducible transcript 4 promotes gastric cancer cell proliferation and tumorigenesis via the MAPK signaling pathway. Additionally, Wu *et al*. [41] demonstrated that calcium release-activated calcium modulator 2 activates MAPK/ERK via FAK, promoting the disassembly of focal adhesions at the rear edge of the cells and enhancing the metastatic ability of gastric cancer cells. Calcium homeostasis is critically involved in the functioning and survival of cells. Calcium ion concentration is tightly controlled by calcium ion-binding proteins in cell organelles and cells for generating and transducing $Ca^{2+}$ signals of various magnitudes in cells [42]. Studies have shown the involvement of calcium signaling in the growth, migration, distant metastasis of cancer cells, inflammation, and survival [43–45].

Furthermore, ZNF proteins have been shown to play significant roles in the immune system, influencing both cellular and humoral immunity [46,47]. Some immune cells, such as mast cells, NKT cells, and NK cells, act as stromal elements within the inflammatory milieu and contribute to human cancer progression [48]. Zhang *et al*. [49] observed a significant increase in effector memory CD4(+)/CD8(+) T cell percentage in the peripheral blood of GC patients compared to healthy controls. Moreover, Mu *et al*. [50] demonstrated that macrophage polarization promotes metastasis and angiogenesis in GC. Additionally, Ammendola *et al*. [51] reported a correlation between mast cell concentration in the cancerous microenvironment and tumor angiogenesis and lymph node involvement. In patients with GC, chymase-positive mast cells are prevalent, and a higher density of these cells is often linked with worse outcomes for the patients [52,53]. Our results revealed a notable elevation in stromal, immune, and ESTIMATE composite scores among patients in the HRG compared to LRG. Furthermore, a significant association was observed between RS and the presence of various immune cells, including mast cells, macrophages, and NKT cells. Thus, our ZNFG signature may serve as a predictive indicator for immune cell infiltration and immune function in GC patients.

However, our study has several limitations. Firstly, our results are based on bioinformatics analyses, and reliability and applicability of the prognostic model need validation with prospective clinical data. Hence, we are in the process of enrolling GC patients to validate and refine our conclusions. Additionally, further experimental studies are required to validate our findings *in vitro* and *in vivo*, which would contribute to a deeper understanding of the roles of ZNFGs in the onset and progression of GC.

## Conclusions

In conclusion, our findings highlight a significant correlation between five ZNFGs and the survival of GC patients. The identified five-ZNFG signature effectively stratified patients into different risk groups, demonstrating its potential as a robust prognostic indicator for GC patients. Notably, the signature was associated with immune cell infiltration and functional differences within the TIME of

GC patients. Therefore, the identified five-ZNFG signature holds promise as molecular biomarker and potential therapeutic target for GC patients.

## Availability of Data and Materials

The data used in this study are available from the corresponding authors upon reasonable request.

## Author Contributions

PFT, QZ, and ZXW designed the research study. PFT, RSH, and YZ conducted bioinformatic analysis, and drafted the manuscript. All authors contributed to important editorial changes in the manuscript. All authors read and approved the final manuscript. All authors have participated sufficiently in the work and agreed to be accountable for all aspects of the work.

## Ethics Approval and Consent to Participate

Not applicable.

## Acknowledgment

Not applicable.

## Funding

This study was funded by the Baoshan District Health Commission Excellent Youth (Yucai) Program (BSWSYC-2023-12).

## Conflict of Interest

The authors declare no conflict of interest.

## References

[1] Sung H, Ferlay J, Siegel RL, Laversanne M, Soerjomataram I, Jemal A, *et al*. Global Cancer Statistics 2020: GLOBOCAN Estimates of Incidence and Mortality Worldwide for 36 Cancers in 185 Countries. CA: A Cancer Journal for Clinicians. 2021; 71: 209–249.

[2] Biondi A, Lirosi MC, D'Ugo D, Fico V, Ricci R, Santullo F, *et al*. Neo-adjuvant chemo(radio)therapy in gastric cancer: Current status and future perspectives. World Journal of Gastrointestinal Oncology. 2015; 7: 389–400.

[3] Russo AE, Strong VE. Gastric Cancer Etiology and Management in Asia and the West. Annual Review of Medicine. 2019; 70: 353–367.

[4] Choi KH, Kim BS, Oh ST, Yook JH, Kim BS. Comparison the sixth and seventh editions of the AJCC staging system for T1 gastric cancer: a long-term follow-up study of 2124 patients. Gastric Cancer. 2017; 20: 43–48.

[5] Laity JH, Lee BM, Wright PE. Zinc finger proteins: new insights into structural and functional diversity. Current Opinion in Structural Biology. 2001; 11: 39–46.

[6] Vilas CK, Emery LE, Denchi EL, Miller KM. Caught with One's Zinc Fingers in the Genome Integrity Cookie Jar. Trends in Genetics. 2018; 34: 313–325.

[7] Minnich M, Tagoh H, Bönelt P, Axelsson E, Fischer M, Cebolla B, *et al*. Multifunctional role of the transcription factor Blimp-1 in coordinating plasma cell differentiation. Nature Immunology. 2016; 17: 331–343.

[8] Cheng A, Guo X, Dai X, Wang Z. Upregulation of ZHX2 predicts poor prognosis and is correlated with immune infiltration in gastric cancer. FEBS Open Bio. 2021; 11: 1785–1798.

[9] Jin XS, Ji TT, Shi ZC, Zhang QQ, Ye FP, Yu WL, *et al*. Knockdown of ZNF479 inhibits proliferation and glycolysis of gastric cancer cells through regulating $\beta$-catenin/c-Myc signaling pathway. The Kaohsiung Journal of Medical Sciences. 2021; 37: 759–767.

[10] Fan L, Tan B, Li Y, Zhao Q, Liu Y, Wang D, *et al*. Silencing of ZNF139-siRNA induces apoptosis in human gastric cancer cell line BGC823. International Journal of Clinical and Experimental Pathology. 2015; 8: 12428–12436.

[11] Li Y, Zhao Q, Fan LQ, Wang LL, Tan BB, Leng YL, *et al*. Zinc finger protein 139 expression in gastric cancer and its clinical significance. World Journal of Gastroenterology. 2014; 20: 18346–18353.

[12] Hu L, Chen M, Dai H, Wang H, Yang W. A Metabolism-Related Gene Signature Predicts the Prognosis of Breast Cancer Patients: Combined Analysis of High-Throughput Sequencing and Gene Chip Data Sets. Oncologie. 2022; 24: 803–822.

[13] Yu G, Wang LG, Han Y, He QY. clusterProfiler: an R package for comparing biological themes among gene clusters. Omics. 2012; 16: 284–287.

[14] Liu TT, Li R, Huo C, Li JP, Yao J, Ji XL, *et al*. Identification of CDK2-Related Immune Forecast Model and ceRNA in Lung Adenocarcinoma, a Pan-Cancer Analysis. Frontiers in Cell and Developmental Biology. 2021; 9: 682002.

[15] Wang S, Su W, Zhong C, Yang T, Chen W, Chen G, *et al*. An Eight-CircRNA Assessment Model for Predicting Biochemical Recurrence in Prostate Cancer. Frontiers in Cell and Developmental Biology. 2020; 8: 599494.

[16] Zhang L, She R, Zhu J, Lu J, Gao Y, Song W, *et al*. Novel lipometabolism biomarker for chemotherapy and immunotherapy response in breast cancer. BMC Cancer. 2022; 22: 1030.

[17] Thrift AP, El-Serag HB. Burden of Gastric Cancer. Clinical Gastroenterology and Hepatology. 2020; 18: 534–542.

[18] Tang S, Lin L, Cheng J, Zhao J, Xuan Q, Shao J, *et al*. The prognostic value of preoperative fibrinogen-to-prealbumin ratio and a novel FFC score in patients with resectable gastric cancer. BMC Cancer. 2020; 20: 382.

[19] Yoon NA, Jo HG, Lee UH, Park JH, Yoon JE, Ryu J, *et al*. Tristetraprolin suppresses the EMT through the down-regulation of Twist1 and Snail1 in cancer cells. Oncotarget. 2016; 7: 8931–8943.

[20] Griseri P, Pagès G. Control of pro-angiogenic cytokine mRNA half-life in cancer: the role of AU-rich elements and associated proteins. Journal of Interferon & Cytokine Research. 2014; 34: 242–254.

[21] Montorsi L, Guizzetti F, Alecci C, Caporali A, Martello A, Atene CG, *et al*. Loss of ZFP36 expression in colorectal cancer correlates to wnt/ ß-catenin activity and enhances epithelial-to-mesenchymal transition through upregulation of ZEB1, SOX9 and MACC1. Oncotarget. 2016; 7: 59144–59157.

[22] Zhu JG, Yuan DB, Chen WH, Han ZD, Liang YX, Chen G, *et al*. Prognostic value of ZFP36 and SOCS3 expressions in human prostate cancer. Clinical & Translational Oncology. 2016; 18: 782–791.

[23] Lyu F, Li Y, Yan Z, He Q, Cheng L, Zhang P, *et al*. Identification of ISG15 and ZFP36 as novel hypoxia- and immune-related gene signatures contributing to a new perspective for the treatment of prostate cancer by bioinformatics and experimental verification. Journal of Translational Medicine. 2022; 20: 202.

Journal of
BIOLOGICAL REGULATORS
and Homeostatic Agents

[24] Chen W, Chen M, Zhao Z, Weng Q, Song J, Fang S, *et al*. ZFP36 Binds With PRC1 to Inhibit Tumor Growth and Increase 5-Fu Chemosensitivity of Hepatocellular Carcinoma. Frontiers in Molecular Biosciences. 2020; 7: 126.

[25] Chen H, Kalaitsidaki M, Warren AC, Avramopoulos D, Antonarakis SE. A novel zinc finger cDNA with a polymorphic pentanucleotide repeat (ATTTT)n maps on human chromosome 19p. Genomics. 1993; 15: 621–625.

[26] Brandenberger R, Wei H, Zhang S, Lei S, Murage J, Fisk GJ, *et al*. Transcriptome characterization elucidates signaling networks that control human ES cell growth and differentiation. Nature Biotechnology. 2004; 22: 707–716.

[27] Takahashi K, Tanabe K, Ohnuki M, Narita M, Ichisaka T, Tomoda K, *et al*. Induction of pluripotent stem cells from adult human fibroblasts by defined factors. Cell. 2007; 131: 861–872.

[28] Liu W, Ma W, Yuan Y, Zhang Y, Sun S. Circular RNA hsa_circRNA_103809 promotes lung cancer progression via facilitating ZNF121-dependent MYC expression by sequestering miR-4302. Biochemical and Biophysical Research Communications. 2018; 500: 846–851.

[29] Luo A, Zhang X, Fu L, Zhu Z, Dong JT. Zinc finger factor ZNF121 is a MYC-interacting protein functionally affecting MYC and cell proliferation in epithelial cells. Journal of Genetics and Genomics. 2016; 43: 677–685.

[30] Donaldson NS, Nordgaard CL, Pierre CC, Kelly KF, Robinson SC, Swystun L, *et al*. Kaiso regulates Znf131-mediated transcriptional activation. Experimental Cell Research. 2010; 316: 1692–1705.

[31] Huang T, Wang YJ, Huang MT, Guo Y, Yang LC, Liu XJ, *et al*. LINC00470 accelerates the proliferation and metastasis of melanoma through promoting APEX1 expression. Cell Death & Disease. 2021; 12: 410.

[32] Cheng Q, Huang C, Cao H, Lin J, Gong X, Li J, *et al*. A Novel Prognostic Signature of Transcription Factors for the Prediction in Patients With GBM. Frontiers in Genetics. 2019; 10: 906.

[33] Klöting N, Wilke B, Klöting I. Triplet repeat in the Repin1 3'-untranslated region on rat chromosome 4 correlates with facets of the metabolic syndrome. Diabetes/Metabolism Research and Reviews. 2007; 23: 406–410.

[34] Heiker JT, Klöting N. Replication initiator 1 in adipose tissue function and human obesity. Vitamins and Hormones. 2013; 91: 97–105.

[35] Sun Y, Sun W, Hua H, Zhang J, Yu Q, Wang J, *et al*. Overexpression of miR-127 Predicts Poor Prognosis and Contributes to the Progression of Papillary Thyroid Cancer by Targeting REPIN1. Hormone and Metabolic Research. 2021; 53: 197–203.

[36] Wang Y, Lin Y. Hsa-mir-127 impairs survival of patients with glioma and promotes proliferation, migration and invasion of cancerous cells by modulating replication initiator 1. Neuroreport. 2018; 29: 1166–1173.

[37] Qi T, Qu J, Tu C, Lu Q, Li G, Wang J, *et al*. Super-Enhancer Associated Five-Gene Risk Score Model Predicts Overall Survival in Multiple Myeloma Patients. Frontiers in Cell and Developmental Biology. 2020; 8: 596777.

[38] Yang SH, Sharrocks AD, Whitmarsh AJ. MAP kinase signalling cascades and transcriptional regulation. Gene. 2013; 513: 1–13.

[39] Wagner EF, Nebreda AR. Signal integration by JNK and p38 MAPK pathways in cancer development. Nature Reviews. Cancer. 2009; 9: 537–549.

[40] Du F, Sun L, Chu Y, Li T, Lei C, Wang X, *et al*. DDIT4 promotes gastric cancer proliferation and tumorigenesis through the p53 and MAPK pathways. Cancer Communications. 2018; 38: 45.

[41] Wu S, Chen M, Huang J, Zhang F, Lv Z, Jia Y, *et al*. ORAI2 Promotes Gastric Cancer Tumorigenicity and Metastasis through PI3K/Akt Signaling and MAPK-Dependent Focal Adhesion Disassembly. Cancer Research. 2021; 81: 986–1000.

[42] Stewart TA, Yapa KTDS, Monteith GR. Altered calcium signaling in cancer cells. Biochimica et Biophysica Acta. 2015; 1848: 2502–2511.

[43] McKeehan WL, Ham RG. Calcium and magnesium ions and the regulation of multiplication in normal and transformed cells. Nature. 1978; 275: 756–758.

[44] Humeau J, Bravo-San Pedro JM, Vitale I, Nuñez L, Villalobos C, Kroemer G, *et al*. Calcium signaling and cell cycle: Progression or death. Cell Calcium. 2018; 70: 3–15.

[45] Prevarskaya N, Skryma R, Shuba Y. Calcium in tumour metastasis: new roles for known actors. Nature Reviews. Cancer. 2011; 11: 609–618.

[46] John SA, Garrett-Sinha LA. Blimp1: a conserved transcriptional repressor critical for differentiation of many tissues. Experimental Cell Research. 2009; 315: 1077–1084.

[47] Maeda T, Merghoub T, Hobbs RM, Dong L, Maeda M, Zakrzewski J, *et al*. Regulation of B versus T lymphoid lineage fate decision by the proto-oncogene LRF. Science. 2007; 316: 860–866.

[48] Sammarco G, Varricchi G, Ferraro V, Ammendola M, De Fazio M, Altomare DF, *et al*. Mast Cells, Angiogenesis and Lymphangiogenesis in Human Gastric Cancer. International Journal of Molecular Sciences. 2019; 20: 2106.

[49] Zhang R, Li F, Li H, Yu J, Ren X. The clinical significance of memory T cells and its subsets in gastric cancer. Clinical & Translational Oncology. 2014; 16: 257–265.

[50] Mu G, Zhu Y, Dong Z, Shi L, Deng Y, Li H. Calmodulin 2 Facilitates Angiogenesis and Metastasis of Gastric Cancer *via* STAT3/HIF-1A/VEGF-A Mediated Macrophage Polarization. Frontiers in Oncology. 2021; 11: 727306.

[51] Ammendola M, Sacco R, Zuccalà V, Luposella M, Patruno R, Gadaleta P, *et al*. Mast Cells Density Positive to Tryptase Correlate with Microvascular Density in both Primary Gastric Cancer Tissue and Loco-Regional Lymph Node Metastases from Patients That Have Undergone Radical Surgery. International Journal of Molecular Sciences. 2016; 17: 1905.

[52] Kondo K, Muramatsu M, Okamoto Y, Jin D, Takai S, Tanigawa N, *et al*. Expression of chymase-positive cells in gastric cancer and its correlation with the angiogenesis. Journal of Surgical Oncology. 2006; 93: 36–42; discussion 42–43.

[53] Lv Y, Zhao Y, Wang X, Chen N, Mao F, Teng Y, *et al*. Increased intratumoral mast cells foster immune suppression and gastric cancer progression through TNF-α-PD-L1 pathway. Journal for Immunotherapy of Cancer. 2019; 7: 54.